Supplementary materials for

Origin of electrolyte-dopant dependent sulfur poisoning of SOFC anodes:

ZhenHua Zeng[1], Mårten E. Björketun[1], Sune Ebbesen[2], Mogens B. Mogensen[2] and Jan Rossmeisl[1*]

[1]*Center for Atomic-Scale Materials Design, Department of Physics,Technical University of Denmark, 2800 Kgs. Lyngby, Denmark*

[2]*Department of Energy Conversion and Storage, DTU Risø Campus, Technical University of Denmark, P.O. Box 49, 4000 Roskilde, Denmark.*

jross@fysik.dtu.dk

S1. Model systems and computational details

To simulate the anode triple phase boundary (TPB) in Ni-*X*SZ (X_2O_3 stabilized zirconia) solid oxide fuel cells (SOFC), we use models of Ni nanorods supported on *X*SZ(111) substrates, as shown in Figures 1 and **Figure S1**. The nanorod is 3 atomic layers in height, 3 atoms wide in the x-direction (infinite length when accounting for periodic boundary conditions), and 2 and 4 atoms wide in the y-direction for top and bottom layers, respectively. Furthermore, the nanorod is (111) terminated in the z-direction, while it exposes two different facets, Ni(111) and Ni(100), on the –y and +y sides of the TPB, a geometry that enables us to study Ni atoms with different reactivity. The *X*SZ(111) substrates are constructed from a ZrO_2(111)-c(2×4) supercell with three O-Zr-O triple layers in the z-direction. This results in a mismatch of -5.8% for Ni in the periodic x-direction. The dopant (X_2O_3) concentration in the *X*SZ substrate is fixed at 9% mol, which corresponds to removing two oxygen atoms from and substituting 4 Zr atoms with *X* atoms in the ZrO_2(111)-c(2×4) supercell. This concentration is in the middle of the normal experimental range of 8% to 10%.[1-3] For Ni-ScSZ (scandia stabilized zirconia) and Ni-YSZ (yttria stabilized zirconia) the models are geometrically optimized for Ni atoms and all possible positions of the cation dopants and O vacancies in the two upper triple layers. The bottom triple layer, which contains only Zr and O, is kept fixed during relaxations. The most stable TPB models located in this screening are shown in Figures 1 and **Figure S1** (the atomic positions in Cartesian coordinates are given in **Table S2** and **Table S3**). For other Ni-*X*SZ systems, structural optimizations start from the most stable Ni-ScSZ and Ni-YSZ models. The energetically most favorable Ni-AlSZ and Ni-GaSZ structures are obtained starting from the Ni-ScSZ configuration, while the most stable Ni-InSZ and Ni-LaSZ systems are derived from Ni-YSZ. The above models are similar to those previously used in DFT calculations on Ni-YSZ and Au-TiO_2.[4, 5] However, the Ni

nanorod used in the present study is wider in the y-direction, and the lowest Ni coordination number is 7 not counting perimeter atoms in contact with the substrate.

S1.1. Ni(100) reconstruction

In the absence of constraints, the clean Ni(100) facet at the TPB reconstructs into a Ni(111) type facet during geometric optimization. The reconstruction is mediated by a shift of the middle row atoms along the x-axis. To prevent the reconstruction and facilitate evaluation of the relative stability with respect to the reconstructed Ni(100) facet, a fix-x-coordinate constraint is applied to one of the middle row atoms. The relative stability, i.e. reconstruction energy (E_{RC}), is defined as:

$$E_{RC} = (E_{tot}(\text{Ni(100)-RC-}X\text{SZ}) - E_{tot}(\text{Ni(100)-}X\text{SZ}))/N \quad \text{(S1)}$$

where E_{tot}(Ni(100)-RC-*X*SZ) and E_{tot}(Ni(100)-*X*SZ) are the total energy of Ni-*X*SZ with a reconstructed and pristine Ni(100) facet, respectively. *N* is the number of Ni atoms on the Ni(100) facet; it is 9 in the present Ni-*X*SZ models.

S1.2. Sulfur adsorption

The original, pristine, Ni(100) facet may be automatically restored upon sulfur adsorption on particular sites of Ni-*X*SZ, e.g. on the HCP11 site of Ni-YSZ. To obtain sulfur adsorption energies on this type of sites a few constrains are set iterantly: first, fix the substrate and optimize only the sulfur position; then release constraints except for the x coordinate of sulfur (the bottom O-Zr-O triple layer is always fixed). The process is repeated until convergence is reached.

The sulfur adsorption energy is defined as:

$$E_{ad} = E_{tot}(\text{S/Ni-}X\text{SZ}) - E_{tot}(\text{S}) - E_{tot}(\text{Ni-}X\text{SZ}) \quad \text{(S2)}$$

and the energy for dissociative adsorption of H_2S is defined as:

$$E_{diss} = E_{tot}(\text{S/Ni-}X\text{SZ}) + E_{tot}(H_2) - E_{tot}(H_2S) - E_{tot}(\text{Ni-}X\text{SZ}) \quad \text{(S3)}$$

where E_{tot}(S), E_{tot}(H_2), E_{tot}(H_2S), E_{tot}(Ni-*X*SZ) and E_{tot}(S/Ni-*X*SZ) are the total energy of S, H_2 and H_2S in a box, of the clean Ni-*X*SZ system and of Ni-*X*SZ with a sulfur adsorbate, respectively. The adsorption energies and dissociative adsorption energies are reported in Table 1 and **Table S1**.

We notice that the absolute adsorption energy is way off for O adsorption if O_2 is used as a reference, because this molecule is notoriously poorly described in standard DFT calculations.[6] However, when using O or H_2O and H_2 as a reference, then the error is much smaller because those atoms and molecules are much better described at the RPBE level.[6, 7] The same principle may apply for S adsorption. Thus, the present scheme,

i.e. using S or H_2 and H_2S not S_2 as references, probably gives the absolute adsorption energies with high quality.

S1.3. Ni-*X*SZ adhesion

Ni is involved in two sequential interactions; first with *X*SZ and then with sulfur. Due to the bonding competition effect, as in the case of coverage dependent adsorption,[8, 9] the first interaction is likely to influence the subsequent interaction/adsorption. This suggests that the Ni-*X*SZ interaction may be used as a descriptor for the sulfur adsorption/poisoning at the TPB of the Ni-*X*SZ anode. To test this idea, the adhesion energy of Ni-*X*SZ, which is the work per unit area required to separate the Ni nanorod from the support, was calculated with the formula

$$W_{adh} = (E_{tot}(\text{Ni}) + E_{tot}(X\text{SZ}) - E_{tot}(\text{Ni-}X\text{SZ}))/A \quad \text{(S4)}$$

where E_{tot}(Ni-*X*SZ) is the total energy of the most stable Ni-*X*SZ models, and E_{tot}(Ni) and E_{tot}(*X*SZ) are the static/unrelaxed total energy of the Ni nanorod and *X*SZ substrate separated from the most stable Ni-*X*SZ, respectively. *A* is the area of Ni(111)-c(3x4) in contact with the *X*SZ support – 61.66 $Å^2$ in this case.

S1.4. Relation between Ni-*X*SZ adhesion and *X*SZ surface energy

The Ni-*X*SZ adhesion energy is closely related to the surface energy of *X*SZ. To study their relation, the surface energies of *X*SZ(111) and ZrO_2(111) are calculated using structures derived from a ZrO_2(111)-(2x2) supercell. The ZrO_2(111) bulk reference is composed of three O-Zr-O triple layers in the z-direction. *X*SZ(111) bulk structures are obtained by introducing one X_2O_3 unit in the first two O-Zr-O triple layers of the ZrO_2 bulk model. This yields the same X_2O_3 concentration as in the Ni-*X*SZ models, i.e. 9%. We note that it is identical for the doping of X_2O_3 in any two of O-Zr-O triple layers in ZrO_2(111) bulk reference due to periodic boundary condition. However, the present setup facilitates surface energy calculations by ensuring that the bottom surface (and its energy) is identical to the pristine ZrO_2 surface, i.e. it separates the total surface energy of *X*SZ into contributions from ZrO_2(111) and *X*SZ(111) (see Eq. S6 below). The bulk structures are optimized using cells of fixed shape and extension in the xy plane, but of variable length in the z-direction. In the case of doped systems, the minimum energy structures were found by carrying out relaxations for all possible distributions of the two X^{3+} cations and the O vacancy. We found that the two X^{3+} prefer to be in different layers, but stay nearest neighbors. The O vacancy prefers a subsurface-like position somewhere in the first O-Zr-O triple layer, but the exact locations depends on the dopants. For AlSZ and GaSZ it coordinates directly with X^{3+}, however, for other *X*SZ's it assumes a position further from X^{3+}.

The surface energy is calculated for both relaxed and static (unrelaxed) surfaces. Static surfaces are obtained by cleaving bulk models and inserting a vacuum layer. The relaxed surfaces of ScSZ and YSZ are obtained by geometric optimization of the first two O-Zr-O triple layers, and by considering all possible distributions of the X^{3+}'s and the O vacancy in those layers. The most favorable distributions of Sc^{3+}/$Y^{3+}$and the O vacancy turn out to be identical to those in the bulk models. Thus, for other systems, we simply start the geometric optimization from static surface models, i.e. those obtained by cleaving the most stable bulk models. The surface energy of ZrO_2 is calculated according to:

$$\gamma(ZrO_2)=(E_{surf}(ZrO_2)-E_{bulk}(ZrO_2))/2 \quad \text{(S5)}$$

where E_{bulk} is the total energy of the bulk model and E_{surf} is the total energy of surface model. The surface energies of *X*SZ's are calculated by subtracting the ZrO_2 part (bottom side of slab) from the total surface energy of *X*SZ:

$$\gamma(XSZ)=\Delta E(XSZ)-\gamma(ZrO_2) \quad \text{(S6)}$$

where $\Delta E(XSZ)$ is the total surface energy of *X*SZ, calculated according to $\Delta E(XSZ)=E_{surf}(XSZ)-E_{bulk}(XSZ)$. We note that, with the current atomic setup, the above formulas will give the surface energies of (2 x 2) unit wide surfaces. To convert to a standard unit, e.g. j/m^2, the area of the surface, i.e. 46.24 $Å^2$, must be considered.

S1.5. DFT details

If nothing else is specified, the density functional theory (DFT) calculations are performed spin-polarized using GPAW, a real-space PAW code,[10, 11] in linear-combination-of-atom-orbitals (LCAO) mode with a double-zeta polarized basis. The density, effective potential, and wave functions (for finite difference (FD) mode) are evaluated on a real space grid with a grid spacing of around 0.18 Å. The exchange-correlation energy is evaluated with an RPBE[12] generalized gradient approximation (GGA) functional. The Brillouin zone (BZ) of cc Ni bulk is sampled with a (12x12x12) Monkhorst-Pack k-point grid, the BZ of cubic ZrO_2 bulk with a (8x8x8) k-point grid (12x1), the BZ's of bulk ZrO_2(111)-(2x2) and *X*SZ(111)-(2x2) with three O-M-O triple layers in the z-direction with a (4x4x3) grid, the BZ's of cleaved ZrO_2(111)-(2x2) and *X*SZ(111)-(2x2) surface supercells with a (4x4x1) grid, the BZ's of Ni-*X*SZ(111)-c(2x4) triple phase boundary models with a (4x2x1) grid, and the BZ's of Ni(111)-(2x2) and Ni(100)-(2x2) surface supercells with a (6x6x1) grid. In the surface calculations, periodically repeated slabs are separated by at least 10 Å of vacuum in the direction perpendicular to the surface. For isolated atoms and molecules we use a (15Åx15Åx15Å) box and only Γ-point Bloch functions. Lattice constants are determined by fitting to an equation of state (EOS).[13] That result in lattice constants of 5.167 Å for ZrO_2 (the experimental values is 5.09 Å[14]); 3.483 Å, 3.595 Å and 3.671 for Ni calculated in LCAO mode, FD mode and FD mode with van der Waals correction (wD-DF2)[15], respectively (the experimental value is 3.52 Å[16]).

During structural optimization, the atomic positions are relaxed until the maximum force is less than 0.02 eV/Å. The nudged elastic band (NEB) method is employed for calculations of reconstruction barriers.[17-19]

S2. Reliability of the present study

The main conclusions in the present work are based on results obtained from DFT calculations performed in LCAO mode. There are two issues that may influence the reliability of the present study. The first one is whether the results from zero-temperature DFT calculations are still valid under SOFC operating conditions as the temperature is usually around 1000 K. The second one is the reliability of the DFT calculations themselves.

The first issue relates to the vibrational entropy (ΔS_{vib}) at high temperature and its influence on the surface free energy and adsorption free energy. When the temperature increases, the vibrational entropy gets larger (see Eq S11) and its contribution ($-\Delta T S_{vib}$) to the surface free energy and the adsorption free energy becomes more important. The vibrational frequencies are slightly different for surface atoms (and adsorbates) on Ni(111) and Ni(100) surfaces. As the entropy of adsorbed S and metal Ni is very small, the vibrational contribution to the entropy difference between Ni(111) and Ni(100) surfaces must be very small. Consequently, even though the surface (adsorption) free energies of both Ni(111) and Ni(100) depend on the temperature, the corresponding difference is only weakly temperature dependent. We thus conclude that the relative stability of Ni(111) and Ni(100) surfaces (i.e. the trends in surface reconstruction), and sulfur adsorption on them, predicted from zero-temperature DFT calculations, are still valid under SOFC operating conditions.

The second issue is about the modes and parameters used in DFT calculations. For LCAO mode, small basis sets are susceptible to basis set superposition errors (BSSE's). As a result there could be an uncertainty related with the conclusions deduced from the sulfur adsorption energies calculated on Ni atoms at the TPB of Ni-*X*SZ. To assess the effect of the BSSE's, we first calculate sulfur adsorption energies on Ni(111) and Ni(100) terraces and correct the energies using the counterpoise method (CP).[20, 21] Calculations performed in FD mode are also used as a benchmark. The results are given in **Table S1**. It is seen that the BSSE's are significant in the present calculations (0.72 eV for adsorption on Ni(111) and 0.87 eV for adsorption on Ni(100)). Actually, even when the BSSE's are accounted for, the adsorption energies still differ slightly from the results obtained in FD mode. However, it is worth noticing that the energy differences between

the adsorption on Ni(111) and Ni(100) are only weakly dependent on the basis set as well as on all other parameters; they range from 0.52 eV to 0.72 eV for all different modes and parameter settings (see **Table S1**). For sulfur adsorption on the TPB, the BSSE's are likely to remain big because of the structural similarity between Ni facets at the TPB and the corresponding terraces. Differences in energy between adsorption on different sites or with respective to adsorption on Ni(111) or Ni(100) are, on the other hand, expected to be fairly independent of settings. Thus, it is more reliable to focus on relative adsorption energies and that is exactly what we do in the present communication, i.e. the adsorption energies are compared with respect to the value on the Ni(111) terrace. (Actually, as discussed in next section, the relative adsorption energy is also more important because it reflects the relative sulfur tolerance of different Ni-*X*SZ anodes.) The reliability of the scheme is further verified by complementary static calculations on typical TPB models within the FD mode (see **Figure S2**); LCAO and FD calculations predict the same trend for relative adsorption energies. Thus, we conclude that even though the LCAO calculations are associated with large BSSE's, the relative sulfur tolerance of different Ni-*X*SZ anodes can be accurately predicted.

S3. Impact of the adsorption energy on the sulfur tolerance

The main source of sulfur poisoning is H_2S. The poisoning mechanism is as follow:

$$H_2S(g)+*\rightarrow S^*+H_2(g) \qquad (S7)$$

The free energy of this reaction is

$$\Delta G=G(S^*)+G(H_2)-G(H_2S)-G(*) \qquad (S8)$$

where G is the Gibbs energy of the substances involved in the reaction, and can be expressed as

$$G=E_{tot}+\mu \qquad (S9)$$

E_{tot} is the total energy, obtained from DFT calculations, $\mu=\Delta H-T\Delta S$ is the chemical potentials. For the molecules in gas phase, μ is taken from standard thermodynamic tables.[22] For the adsorbed sulfur atoms, μ is calculated using the vibrational frequencies in Ref.[23] with the below formula.[23 24]

$$\Delta H = R\sum_i \left(\frac{\tau_i}{2}+\frac{\tau_i}{\exp(\tau_i/T)-1}\right) \qquad (S10)$$

$$\Delta S = R\sum_i \left(\frac{\tau_i/T}{\exp(\tau_i/T)-1} - \ln(1-\exp(-\tau_i/T))\right) \quad \text{(S11)}$$

Where R is gas constant, and τ is the vibrational temperature.

Using the above expressions, the Eq. S8 can be rewritten as

$$\Delta G = \Delta\mu_{H2S} - E_{diss} \quad \text{(S12)}$$

E_{diss} is H_2S dissociative adsorption energy as given in Eq. S3, $\Delta\mu_{H2S}$ is the chemical potential of H_2S with respect to dissociated H_2S (H2 and S*) and is calculated with

$$\Delta\mu_{H2S} = \mu_{H2S} - \mu_{S^*} - \mu_{H2} \quad \text{(S13)}$$

The dissociative adsorption energies on Ni(111) and Ni(100) surfaces, and the chemical potentials of H_2S with respect to dissociated H_2S and at different conditions are plotted in **Figure S3**.

The diagram provides a way to roughly estimate the sulfur tolerance of Ni(111), Ni(100) or Ni-*X*SZ at a given set of conditions by comparing E_{diss} and $\Delta\mu_{H2S}$, and the free energy of the reaction, ΔG, in Eq. S12. For example, on Ni(111) the highest tolerable H_2S concentration at 1200 K seems to be about 0.1 ppm, which according to adsorption kinetics ($\theta_S = 1/(1+\exp((E_{diss}-\Delta\mu)/k_BT))$) would yield an equilibrium sulfur coverage of 7.7%. On Ni(100), on the other hand, 0.1 ppm H_2S would probably be too much even at 1500 K and result in an equilibrium sulfur coverage of 11%. Due to the uncertainty in the calculated adsorption energies (see **Table S1**), the predicted coverages might have a large error bar. However, the trend should be correct since calculated differences in adsorption energies are much more accurate. Stronger dissociative adsorption, e.g. on Ni(100) compared to Ni(111), means the poisoning problem will be more severe and stricter control of the operating conditions is needed e.g. higher temperature or lower H_2S concentration. Therefore, it should be possible to use **Figure S3** to estimate the relative sulfur tolerance of different Ni-*X*SZ anodes.

From **Figure S3** we see that the chemical potential of H_2S changes approximately 0.15 eV per 100 K or 0.2 eV per 120-150K. Focusing on the trend at 1000 K, we see that an order of magnitude change in the H_2S concentration, e.g. from 0.1ppm ($\Delta\mu$=-1.8 eV) to 1 ppm ($\Delta\mu$=-1.6 eV) or from 1 ppm to 10 ppm ($\Delta\mu$=-1.4 eV), corresponds to a 0.2 eV

246 change in chemical potential (it would be larger at higher temperature due to larger
247 contribution of H_2S than H_2 and S*). This means that if the sulfur adsorption on the TPB
248 of a given Ni-*X*SZ is 0.2 eV weaker than on the TPB of another anode, e.g. Ni-YSZ, the
249 same sulfur tolerance can be achieved at a 120-150 K lower operating temperature; or
250 the sulfur tolerance can be improved by 1 order of H_2S concentration at around 1000 K
251 or higher temperature.

252

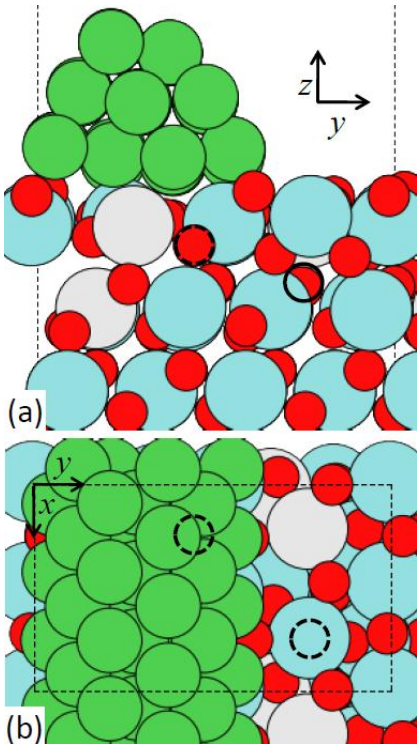

Figure S1 Model of the Ni-ScSZ TPB. See Figure 1 for details and explanation. The Sc atoms are denoted by white balls.

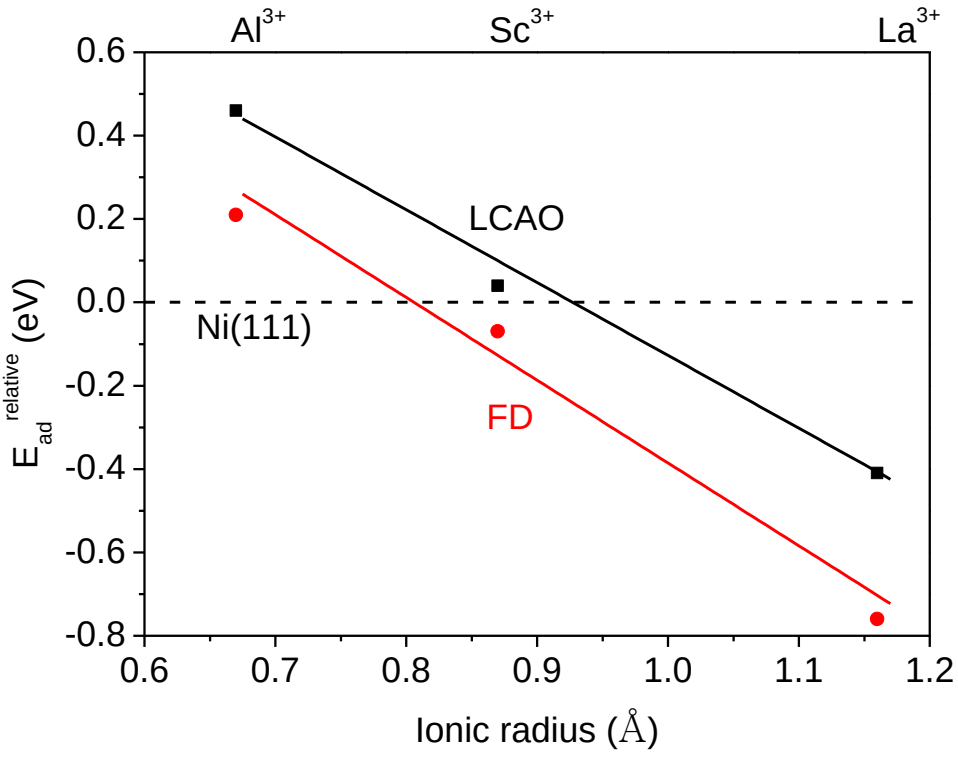

261

262 Figure S2 Trend in relative adsorption energy obtained with LCAO and FD calculations.

263

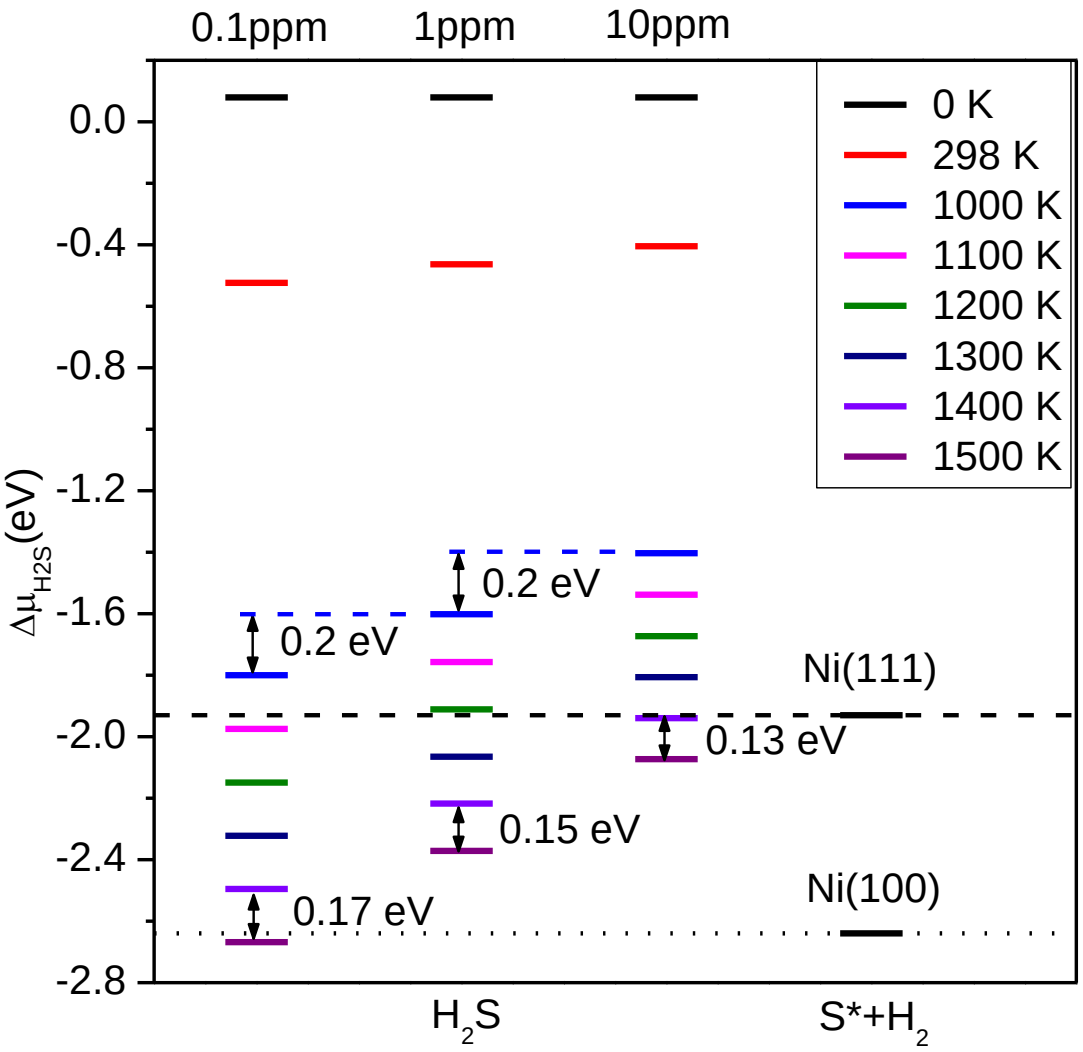

264

265 Figure S3 Chemical potential of H_2S with respect to dissociated H_2S (H_2 and S*) at a few
266 relevant temperatures and concentrations.

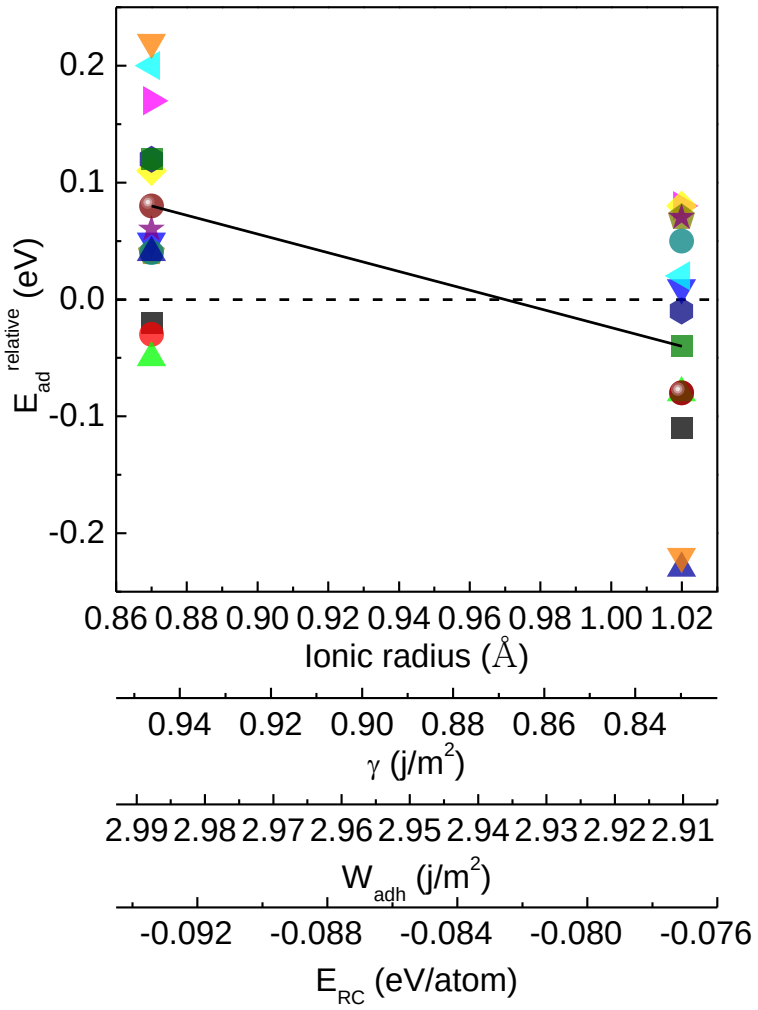

Figure S 4 Sulfur adsorption energies on ScSZ and YSZ. The adsorption energies are plotted versus several parameters: the X^{3+} radius; the surface energy (γ) of *X*SZ; the adhesion energy (W_{adh}) of Ni-*X*SZ; and the reconstruction energy (E_{RC}) of the Ni(100) facet. The line indicates the change in average adsorption energy from ScSZ to YSZ.

Table S1 sulfur adsorption energy and H_2S dissociative adsorption energy on Ni(111) and Ni(100) surfaces, calculated with different DFT codes and/or setups. The reaction energies of $S(g)+H_2(g)\rightarrow H_2S(g)$ are -3.20 eV in LCAO mode, –3.13 eV in FD mode, and -2.92 eV in FD model with van der Waals correction, respectively.

				E_{ad}^{S} (eV)		$E_{dis}^{H_2S}$ (eV)		
code	Basis sets	XC	Spin[a]	Ni(111)	Ni(100)	Ni(111)	Ni(100)	Ref.
GPAW	LCAO	RPBE	True	-5.14	-5.84	-1.93	-2.64	Present work
GPAW	LCAO-BSSE	RPBE	True	-4.42	-4.97	-1.21	-1.76	Present work
GPAW	Grid-FD	RPBE	True	-4.61	-5.28	-1.43	-2.15	Present work[b]
GPAW	Grid-FD	RPBE	True	-4.77	-5.33	-1.64	-2.20	Present work
GPAW	Grid-FD	RPBE	False	-4.99	-5.68	-1.86	-2.55	Present work
GPAW	Grid-FD	vdW-DF2	True	-4.64	-5.16	-1.72	-2.24	Present work
GPAW	Grid-FD	RPBE	False			-1.76		[23]
VASP	Plane wave	PBE	Unknown	-5.29	-5.97	-1.96	-2.64	[25]
VASP	Plane wave	PBE	True	-5.31				[26]
VASP	Plane wave	PW91	True	-5.16				[27]
VASP	Plane wave	PW91	False			-1.75		[28]

[a]Spin-polarized or spin-paired calculation refers to the TPB species; gas-phase atoms/molecules are always subject to spin-polarized treatment.

[b]The calculations were performed on LCAO optimized structures without further relaxation.

286

287

288 Table S2 Cartesian coordinates of a Ni-YSZ model in a (7.307241 Å, 12.656514 Å,
289 23.483351 Å) orthorhombic cell.

No.	element	x (Å)	y (Å)	z (Å)
1	Zr	1.8268	1.0547	5.7458
2	Zr	5.4804	1.0547	5.7458
3	Zr	0	4.2188	5.7458
4	Zr	3.6536	4.2188	5.7458
5	Zr	1.8268	7.383	5.7458
6	Zr	5.4804	7.383	5.7458
7	Zr	0	10.5471	5.7458
8	Zr	3.6536	10.5471	5.7458
9	Zr	-0.01711	2.15198	8.74171
10	Zr	3.67069	2.15232	8.74187
11	Zr	5.48005	5.18914	8.59744
12	Zr	-0.12361	8.3548	8.71949
13	Zr	3.77625	8.35468	8.71973
14	Zr	1.82765	11.77374	8.62617
15	Zr	0.00238	-0.11103	11.6964
16	Zr	3.65061	-0.11269	11.6954
17	Zr	5.47875	2.94398	11.93106
18	Zr	0.12986	6.58381	11.76334
19	Zr	3.52121	6.58458	11.76333
20	Zr	1.82782	9.69939	12.08754
21	Y	1.82721	3.33388	11.80782
22	Y	5.48112	11.57313	8.74185
23	Y	1.82673	5.29036	8.78561
24	Y	5.48138	9.58366	11.83727
25	O	1.8268	5.2735	6.4916
26	O	5.4804	5.2735	6.4916
27	O	0	8.4377	6.4916
28	O	3.6536	8.4377	6.4916
29	O	1.8268	11.6018	6.4916
30	O	5.4804	11.6018	6.4916
31	O	0	2.1094	6.4916
32	O	3.6536	2.1094	6.4916
33	O	-0.31068	6.30779	9.63057

34	O	3.96335	6.30719	9.63079
35	O	5.48046	9.32689	9.53237
36	O	0.09749	12.75985	9.51515
37	O	3.55702	12.75901	9.51465
38	O	1.82654	3.09276	9.53649
39	O	5.48011	3.27378	9.62024
40	O	-0.4396	4.57997	11.98911
41	O	4.08755	4.57818	11.98937
42	O	1.82599	7.67483	12.93793
43	O	5.47951	7.34592	12.21691
44	O	0.0582	10.60917	12.74906
45	O	3.59628	10.60986	12.74856
46	O	1.82779	0.37522	12.62148
47	O	5.47871	0.62711	12.87697
48	O	1.8268	3.1641	5
49	O	5.4804	3.1641	5
50	O	0	6.3283	5
51	O	3.6536	6.3283	5
52	O	1.8268	9.4924	5
53	O	5.4804	9.4924	5
54	O	0	0	5
55	O	3.6536	0	5
56	O	-0.03125	4.18769	7.92094
57	O	3.68464	4.18777	7.92067
58	O	1.82652	7.55682	8.16378
59	O	5.48035	7.36704	7.85317
60	O	0.18626	10.42726	8.07245
61	O	3.46767	10.42741	8.07251
62	O	1.82684	1.10606	7.88709
63	O	5.4806	1.17093	7.97397
64	O	-0.05993	1.99536	11.21294
65	O	3.71234	1.99429	11.21164
66	O	1.82566	5.56624	11.07188
67	O	0.38761	8.57398	10.83271
68	O	3.26506	8.57361	10.83259
69	O	1.82699	11.22117	10.70125
70	O	5.48092	11.61518	10.97217
71	Ni	1.82497	0.778	14.51796
72	Ni	4.26617	0.81534	14.5775
73	Ni	6.6898	0.81451	14.5748

74	Ni	0.623	2.83311	14.36398
75	Ni	3.02622	2.83283	14.36384
76	Ni	5.47915	2.85227	14.44832
77	Ni	1.82376	4.9289	14.30855
78	Ni	4.21827	4.87754	13.98706
79	Ni	6.73727	4.87821	13.98712
80	Ni	0.6051	7.02155	14.46374
81	Ni	3.04361	7.02128	14.46446
82	Ni	5.47771	6.93623	14.22848
83	Ni	0.61328	1.58561	16.48799
84	Ni	3.03432	1.58415	16.4883
85	Ni	5.47857	1.61093	16.56496
86	Ni	1.82391	3.69135	16.28265
87	Ni	4.24205	3.74911	16.20929
88	Ni	6.71528	3.74922	16.20866
89	Ni	1.82471	6.13618	16.41024
90	Ni	4.27638	6.07262	16.18358
91	Ni	6.68117	6.07311	16.18311
92	Ni	1.82494	2.70946	18.35401
93	Ni	4.2524	2.731	18.31477
94	Ni	6.70371	2.73089	18.31439
95	Ni	0.58796	4.83732	17.97914
96	Ni	3.06159	4.83671	17.97898
97	Ni	5.4783	4.83908	17.94159

290

291

292

293

294 Table S3 Cartesian coordinates of a Ni-ScSZ model in a (7.307241 Å, 12.656514 Å,
295 23.483351 Å) orthorhombic cell.

No.	element	x (Å)	y (Å)	y (Å)
1	Zr	1.8268	1.0547	5.7458
2	Zr	5.4804	1.0547	5.7458
3	Zr	0	4.2188	5.7458
4	Zr	3.6536	4.2188	5.7458
5	Zr	1.8268	7.383	5.7458
6	Zr	5.4804	7.383	5.7458
7	Zr	0	10.5471	5.7458
8	Zr	3.6536	10.5471	5.7458
9	Zr	-0.00146	2.16182	8.61142
10	Zr	1.81393	5.19698	8.59187
11	Zr	5.47305	5.23541	8.73304
12	Zr	3.56064	8.26679	8.6702
13	Zr	1.99169	11.45534	8.64802
14	Zr	5.55693	11.83529	8.62753
15	Zr	-0.10332	-0.12192	11.80786
16	Zr	3.48147	-0.2093	11.65041
17	Zr	1.82888	3.01634	11.84774
18	Zr	-0.08083	6.63411	11.65941
19	Zr	3.81686	6.61131	11.71795
20	Zr	5.44881	9.68464	11.96341
21	Sc	3.59196	2.08581	8.68687
22	Sc	0.14489	8.32927	8.67318
23	Sc	5.24911	3.40176	11.61255
24	Sc	1.56684	9.62418	11.57331
25	O	1.8268	5.2735	6.4916
26	O	5.4804	5.2735	6.4916
27	O	0	8.4377	6.4916
28	O	3.6536	8.4377	6.4916
29	O	1.8268	11.6018	6.4916
30	O	5.4804	11.6018	6.4916
31	O	0	2.1094	6.4916
32	O	3.6536	2.1094	6.4916
33	O	0.25805	6.28594	9.52248

34	O	3.38829	6.23791	9.56277
35	O	1.9115	9.37873	9.43681
36	O	-0.33209	13.11385	9.7479
37	O	3.66922	12.64464	9.4775
38	O	1.69541	3.18777	9.5681
39	O	5.56294	3.22053	9.55423
40	O	0.70943	4.75211	11.82055
41	O	3.36152	4.53471	11.85166
42	O	1.90391	7.52759	12.08702
43	O	5.50579	7.66762	12.85108
44	O	0.00207	10.50404	12.6577
45	O	3.45934	10.39667	12.33262
46	O	1.82969	0.35216	12.83046
47	O	5.29608	-0.19919	12.69348
48	O	1.8268	3.1641	5
49	O	5.4804	3.1641	5
50	O	0	6.3283	5
51	O	3.6536	6.3283	5
52	O	1.8268	9.4924	5
53	O	5.4804	9.4924	5
54	O	0	0	5
55	O	3.6536	0	5
56	O	-0.05077	4.25276	7.88085
57	O	3.685	4.20206	7.95261
58	O	1.84433	7.33112	7.84307
59	O	5.48251	7.39366	8.06922
60	O	-0.02773	10.62123	8.05538
61	O	3.79409	10.48025	8.00487
62	O	1.77362	1.00563	7.96793
63	O	5.45501	1.1337	7.85909
64	O	-0.20725	2.10997	11.90872
65	O	3.6445	1.95894	11.22348
66	O	5.52768	5.55745	10.91662
67	O	-0.26953	8.60163	10.78719
68	O	4.29868	8.42339	10.61817
69	O	1.58148	11.60537	10.71386
70	O	5.60234	11.0726	10.52505
71	Ni	0.68867	0.66566	14.52902
72	Ni	3.09954	0.66677	14.50747
73	Ni	5.53638	0.62423	14.42331

74	Ni	-0.5159	2.67973	13.9448
75	Ni	1.93247	2.69932	14.29462
76	Ni	4.36137	2.68432	14.15648
77	Ni	0.69028	4.8111	13.83868
78	Ni	3.18512	4.77608	13.87559
79	Ni	5.59933	4.81357	14.06264
80	Ni	-0.5449	6.92586	14.33248
81	Ni	1.90857	6.87875	14.07078
82	Ni	4.33794	6.91293	14.35156
83	Ni	-0.5589	1.49592	16.31323
84	Ni	1.89005	1.49665	16.4608
85	Ni	4.33062	1.48074	16.35967
86	Ni	0.63271	3.59587	15.97922
87	Ni	3.14813	3.60165	16.05485
88	Ni	5.57083	3.55176	16.01148
89	Ni	0.68701	5.93791	16.02327
90	Ni	3.07522	5.94723	16.03817
91	Ni	5.53509	5.96459	16.21768
92	Ni	0.65587	2.62069	18.1512
93	Ni	3.11168	2.61108	18.19634
94	Ni	5.53831	2.61045	18.15419
95	Ni	-0.53072	4.68745	17.77054
96	Ni	1.88176	4.68527	17.75186
97	Ni	4.31098	4.69334	17.7922

296

297

References

1. Z. Cheng, J.-H. Wang, Y. Choi, L. Yang, M. C. Lin and M. Liu, *Energy Environ. Sci.*, 2011, **4**, 4380-4409.
2. K. Sasaki, K. Susuki, A. Iyoshi, M. Uchimura, N. Imamura, H. Kusaba, Y. Teraoka, H. Fuchino, K. Tsujimoto, Y. Uchida and N. Jingo, *J. Electrochem. Soc.*, 2006, **153**, A2023-A2029.
3. K. V. Hansen and M. Mogensen, *Electrochem. Solid-State Lett.*, 2012, **15**, B70-B71.
4. M. Shishkin and T. Ziegler, *J. Phys. Chem. C*, 2009, **113**, 21667-21678.
5. I. X. Green, W. J. Tang, M. Neurock and J. T. Yates, *Science*, 2011, **333**, 736-739.
6. S. Kurth, J. P. Perdew and P. Blaha, *Int. J. Quantum Chem.*, 1999, **75**, 889-909.
7. J. I. Martinez, H. A. Hansen, J. Rossmeisl and J. K. Nørskov, *Phys. Rev. B*, 2009, **79**, 045120.
8. J. R. Kitchin, *Phys. Rev. B*, 2009, **79**, 205412.
9. E. Skúlason, V. Tripkovic, M. E. Björketun, S. d. Gudmundsdóttir, G. Karlberg, J. Rossmeisl, T. Bligaard, H. Jónsson and J. K. Nørskov, *J. Phys. Chem. C*, 2010, **114**, 18182-18197.
10. J. J. Mortensen, K. Kaasbjerg, S. L. Frederiksen, J. K. Nørskov, J. P. Sethna and K. W. Jacobsen, *Phys. Rev. Lett.*, 2005, **95**, 216401.
11. J. J. Mortensen, L. B. Hansen and K. W. Jacobsen, *Phys. Rev. B*, 2005, **71**, 035109.
12. B. Hammer, L. B. Hansen and J. K. Nørskov, *Phys. Rev. B*, 1999, **59**, 7413-7421.
13. A. B. Alchagirov, J. P. Perdew, J. C. Boettger, R. C. Albers and C. Fiolhais, *Phys. Rev. B*, 2003, **67**, 026103.
14. M. Shishkin and T. Ziegler, *J. Phys. Chem. C*, 2008, **112**, 19662-19669.
15. K. Lee, É. D. Murray, L. Kong, B. I. Lundqvist and D. C. Langreth, *Phys. Rev. B*, 2010, **82**, 081101.
16. C. Kittel, *Introduction to Solid State Physics*, 8th edn., John Wiley & Sons, 2004.
17. H. Jonsson, G. Mills and K. W. Jacobsen, *Classical and Quantum Dynamics in Consensed Phase Simulations*, World Scientific, Singapore, 1998.
18. G. Henkelman and H. Jonsson, *J. Chem. Phys.*, 2000, **113**, 9978-9985.
19. G. Henkelman, B. P. Uberuaga and H. Jonsson, *J. Chem. Phys.*, 2000, **113**, 9901-9904.
20. F. B. van Duijneveldt, J. G. C. M. van Duijneveldt-van de Rijdt and J. H. van Lenthe, *Chem Rev*, 1994, **94**, 1873-1885.
21. B. Paizs and S. Suhai, *J. Comput. Chem.*, 1998, **19**, 575-584.
22. M. W. Chase, *NIST-JANAF Thermochemical Tables*, 4th edn., American Chemical Society, Woodbury, N.Y., 1998.
23. D. S. Monder and K. Karan, *J. Phys. Chem. C*, 2010, **114**, 22597-22602.
24. J. Rossmeisl and W. G. Bessler, *Solid State Ionics*, 2008, **178**, 1694-1700.
25. J.-H. Wang and M. Liu, *Electrochem. Commun.*, 2007, **9**, 2212-2217.
26. D. R. Alfonso, *Surf. Sci.*, 2008, **602**, 2758-2768.
27. E. J. Albenze and A. Shamsi, *Surf. Sci.*, 2006, **600**, 3202-3216.
28. Y. M. Choi, C. Compson, M. C. Lin and M. Liu, *Chem. Phys. Lett.*, 2006, **421**, 179-183.